processes

MDPI

Article

Numerical Analysis of Cracking Processes in RC Beams without Transverse Reinforcement

Piotr Smarzewski [1,*] and Marta Słowik [2]

[1] Faculty of Civil Engineering and Geodesy, Military University of Technology, 2 gen. Sylwestra Kaliskiego, 00-908 Warsaw, Poland
[2] Department of Structural Engineering, Faculty of Civil Engineering and Architecture, Lublin University of Technology, 40 Nadbystrzycka, 20-618 Lublin, Poland
* Correspondence: piotr.smarzewski@wat.edu.pl; Tel.: +48-698695284

Abstract: The procedure of FEM calculations was presented in the paper. The numerical calculations concerned a simulation of crack distribution and propagation in concrete beams reinforced longitudinally without shear reinforcement. The analysis of the obtained FEM results showed different modes of failure in the beams when shear span-to-depth ratio was a/d = 2.5 and a/d = 1.8. In the analyzed beams, the ratio of longitudinal reinforcement and the mechanical properties of the steel bars were also changing parameters. The FEM results have showed that the shear failure of reinforced concrete beams without transverse reinforcement significantly depends on the ratio and yield strength of longitudinal steel bars. Furthermore, the results of numerical calculation for the beams of a/d = 2.5 were also juxtaposed with experiments performed by the author on two longitudinally reinforced concrete beams.

Keywords: reinforced concrete beams; cracks distribution; numerical analysis

Citation: Smarzewski, P.; Słowik, M. Numerical Analysis of Cracking Processes in RC Beams without Transverse Reinforcement. *Processes* **2023**, *11*, 584. https://doi.org/10.3390/pr11020584

Received: 31 December 2022
Revised: 11 February 2023
Accepted: 12 February 2023
Published: 15 February 2023

1. Introduction

Different modes of failure in longitudinally reinforced concrete beams according to the ratio of longitudinal reinforcement were described by Słowik [1]. In slightly reinforced concrete beams, brittle failure is observed due to the quick opening of flexural cracks in the mid-span of the beam. In flexural concrete members with typical ratio of longitudinal reinforcement, inclined cracks can be observed in the support zones where shear forces predominate. In the case of beams without transverse reinforcement, the inclined cracks can cause a dangerous "shear failure".

Several researchers, for example, Walraven [2], Słowik [3], and Carpinteri et al., performed experimental investigations on a shear failure in reinforced concrete members without transverse reinforcement. [4]. It was observed that the character of failure and the cracks' patterns in the investigated beams without stirrups were significantly dependent on the shear span-to-depth ratio a/d and the size of the member.

The shear span-to-depth ratio is considered as the primary parameter that affects shear failure mechanism [5,6]. The broad scale experiments performed by Kani [6] showed significantly higher ultimate shear stress at failure ν_u in flexural beams without transverse reinforcement when shear span-to-depth ratio was lower than 2.5. The decrease in ν_u with the increase in a/d, which was worked out on the basis of test results presented in [6], is shown in Figure 1.

Taking into account the shear capacity and the mode of failure, flexural members are usually divided on the basis of the shear span-to-depth ratio on slender beams when $a/d \geq 2.5$ and short beams when $a/d < 2.5$. Different design methods are used to estimate the sheer carrying capacity of these two groups of members. Strut-and-tie models are used for designing short beams, whereas the shear capacity of slender beams is commonly calculated on the basis of a sectional model. Shear design methods were described in depth

by Bentz [7], and a review of approaches for designing slender beams against shear was given recently by Keskin and Arslan [8]. The early numerical simulations performed by Słowik and Nowicki [9] have confirmed that the shear span-to-depth ratio influences the crack distribution significantly.

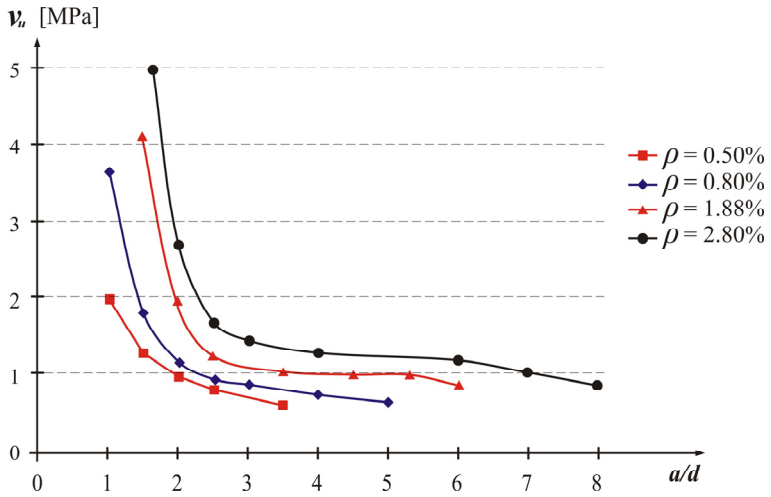

Figure 1. The influence of shear span-to-depth ratio on shear capacity on the basis of test results presented in [6].

The size of the member is another important parameter which must be taken into account when analyzing the failure process in flexural concrete beams. The "size effect in shear" is often defined in literature as the decrease in shear capacity of reinforced concrete beams with the increase in a member depth. Such definition was demonstrated in several papers [10–19]. To illustrate the size effect in shear, test results obtained by Bažant and Kazemi [11] are presented in Figure 2.

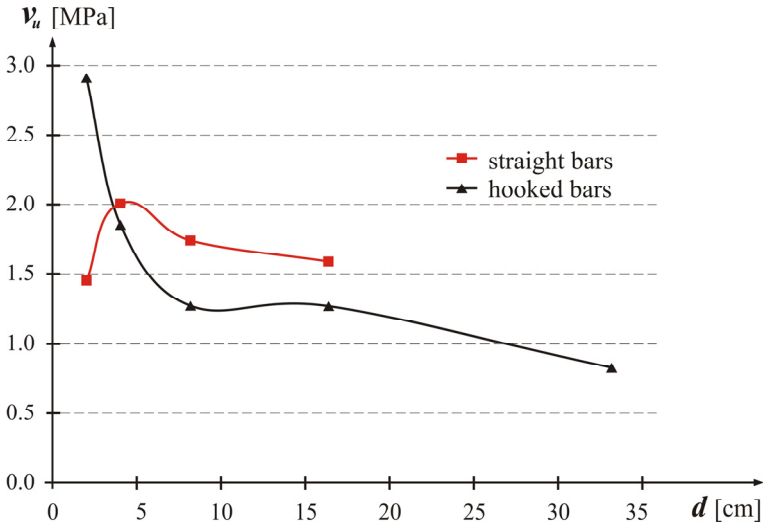

Figure 2. The influence of the beam's depth on shear capacity on the basis of test results presented in [11].

The important role of shear strength and the character of failure in beams without transverse reinforcement plays also in the bond of longitudinal steel bars [11,20] as it can be observed when analyzing test results presented in Figure 2. In the beam with the straight bars and smallest depth, the failure was caused by the loss of bond and flexure, and that type of failure caused a lower load capacity in the beam compared to the shear

capacity in other beams with straight bars. The nonlinear analysis carried out by Słowik and Smarzewski [21] has shown that members characterized by the same shear span-to-depth ratio but different effective length-to-depth ratio can fail in a different way as well.

The influence of longitudinal steel bars on shear failure in beams without stirrups has not been investigated at length in comparison to the effect of sizes. In the experimental investigation performed by Shuaib and Lue [22], the change in ultimate shear stress at failure was observed when longitudinal reinforcement varied in flexural beams. The influence of the reinforcement ratio on shear capacity was seen more significantly in the beams with the shear span-to-depth ratio a/d = 1.0 and a/d = 2.0 (see Figure 3).

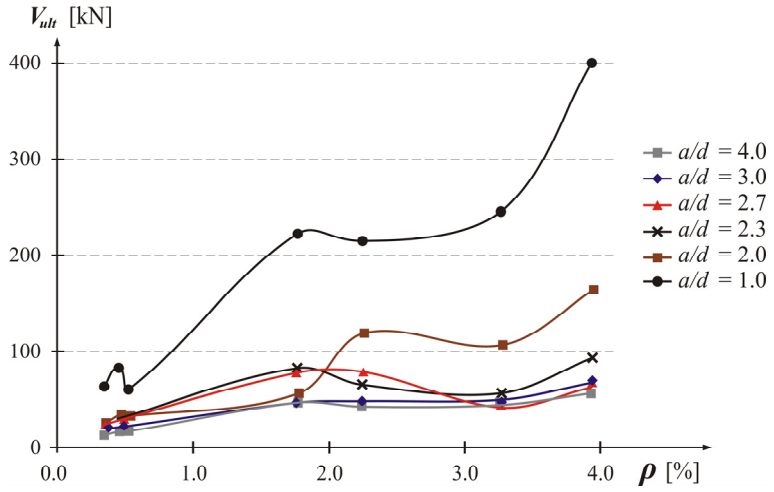

Figure 3. The influence of the longitudinal reinforcement ratio on shear capacity on the basis of test results presented in [22].

The question arises whether the longitudinal reinforcement affects crack distribution and failure process in short beams as well. In this paper, the numerical analysis of the crack evaluation in short longitudinally RC beams without transverse reinforcement is presented. On the basis of the performed FEM analysis, the transition of the failure mechanism according to the shear span-to-depth ratio is demonstrated, and the influence of longitudinal reinforcement on a distribution of cracks is discussed.

2. Materials and Methods

The author's own experimental investigation was performed to analyze the influence of longitudinal reinforcement on load carrying capacity and crack distribution in flexural members without shear reinforcement. A three-point bending test was realized during the experiment. Two longitudinally reinforced concrete beams were tested and the effective span during the test was l_{eff} = 1.1 m. The beams had the rectangular cross-section of the width b = 0.12 m, the total depth h = 0.25 m, and the effective depth d = 0.22 m. As the load was applied in the middle of the span, the shear span-to-depth ratio was a/d = 2.5. The beams differed according to the longitudinal reinforcement. In both investigated members, the reinforcement consisted of two longitudinal steel bars. In the first S3k beam the diameter of bars was 18 mm. The diameter of bars in the PII-3 beam was 12 mm. The geometrical characteristic of tested beams is presented in Figure 4.

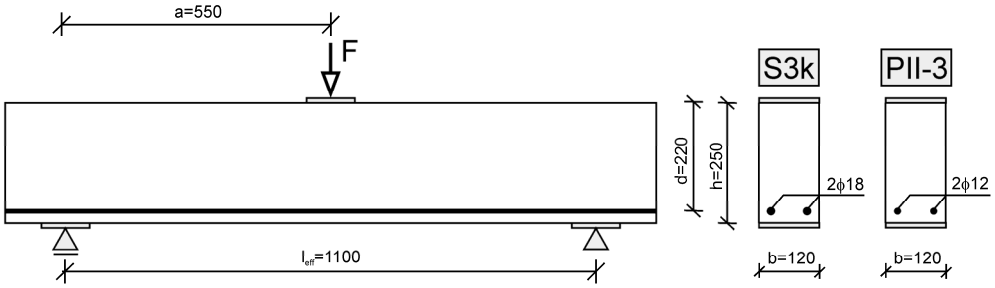

Figure 4. Details of test beams (unit in mm).

The reinforcement ratio in the S3k beam was ρ = 1.8%, and the steel was of the 34GS category; whereas the reinforcement ratio in the PII-3 beam was ρ = 0.9%, and the steel was of the RB500 category. The mechanical properties of the steel bars were tested during the tensile tests. The obtained results are presented in Table 1. The beams were made from a concrete mixture that consisted of: a dolomite coarse aggregate with a maximum diameter of 16 mm—1278 kg/m^3, sand—450 kg/m^3, cement CEM I 32.5R—475 kg/m^3, and water—183 L/m^3. The cylindrical specimens ϕ150/300 mm were prepared from the concrete mixture for testing compressive and tensile strength and the Young's modulus of concrete. The concrete properties obtained from the tests are presented in Table 2.

Table 1. Mechanical properties of reinforcing steel.

Steel	Diameter (mm)	Number of Specimens	Yield Stress, f_y (MPa)		Tensile Strength, f_t (MPa)	
			Mean Value	Standard Deviation	Mean Value	Standard Deviation
34GS	18	10	453	5.1	698	7.2
RB500	12	8	548	3.8	654	5.8

Table 2. Mechanical properties of concrete.

Property	Number of Specimens	Mean Value (MPa)	Standard Deviation (MPa)
Compressive strength, f_c	27	35.0	5.6
Tensile splitting strength, $f_{ct,sp}$	32	3.5	0.4
Young's modulus, E_c	19	41400	3650

Both of the tested beams failed in shear in the support region as the result of the main diagonal crack propagation. The bond of steel bars was monitored during the experiment and the loss of bond in the tested beams was not observed. The instrumentation for bond checking is presented in Figure 5. Although the type of failure was the same in the beams, the shear capacity and cracks distribution differed. When analyzing the load carrying capacity of the investigated beams, a higher ultimate shear force of *Vult* = 51.0 kN was measured in beam S3k with ρ = 1.8% compared to the shear force of *Vult* = 43.5 kN obtained in beam PII-3 with ρ = 0.9%.

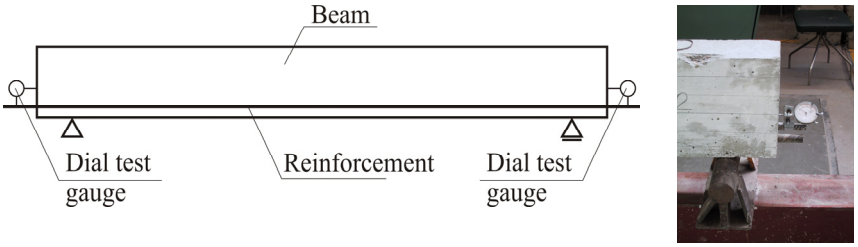

Figure 5. The instrumentation for bond checking.

The development of crack patterns was monitored during the test. In both beams, the first flexural cracks appeared at the beginning of the loading stages in the middle of the span. Following this, some of the perpendicular cracks started to change their orientation towards the applied load. Finally, the main diagonal crack appeared at one side of the beam, which caused the sudden brittle failure of the member. Some differences in crack evaluation were observed during the test according to the longitudinal reinforcement. In beam PII-3, the inclined failure crack developed from the flexural crack, whereas in beam S3k the failure crack formed as the inclined crack. Furthermore, in beam PII-3, with the lower reinforcement ratio, the flexural cracks quickly propagated very deep through the cross section. The quick growth of cracks caused a more sudden failure and a lower capacity in beam PII-3 compared to beam S3k. The crack patterns for both tested beams are presented in Figure 6.

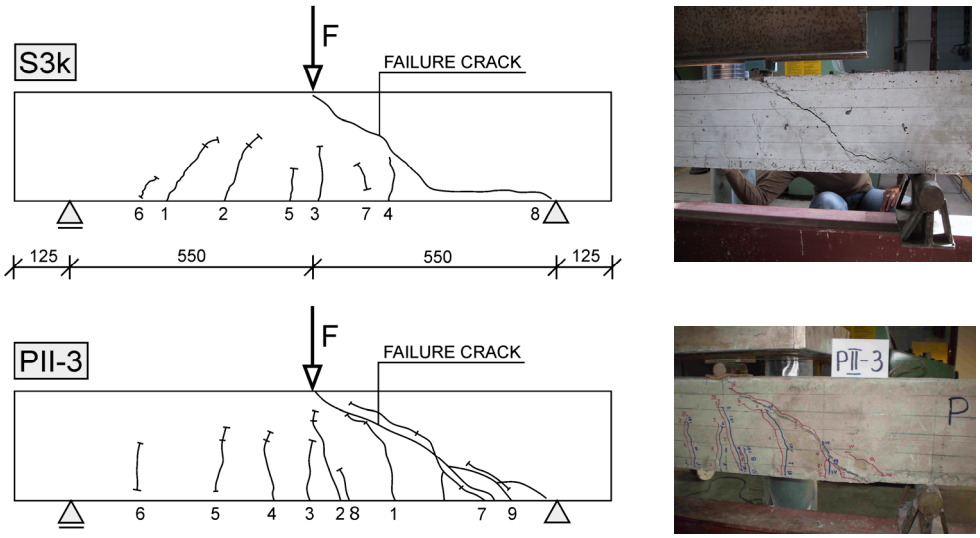

Figure 6. Cracks patterns for the slender beams S3k (2ϕ18) and PII-3 (2ϕ12).

When analyzing the character of failure, the tested beams can be considered as slender beams. Numerical simulations were performed to analyze the crack distribution in both the slender beams and short beams. As the yield stress of steel bars in the two tested beams was different, it was not possible to conclude if the reinforcement was the only parameter influencing the shear capacity and crack distribution, or if steel properties were also of importance. The aim of this analysis is to answer the question of whether the development of cracks depends only on the amount of reinforcement or on the steel's properties as well.

In the numerical investigations, two types of beams were modeled: a beam of l_{eff} = 1.1 m corresponding to the tested members and a beam of l_{eff} = 0.9 m. All other parameters in the FEM simulation were kept the same as during the experiment: the dimensions of cross sections, the static scheme of the beams, the type of load (simply supported beam loaded by a concentrated force), material properties, and reinforcing steel bars 2ϕ12 or 2ϕ18. The specimens analyzed in FEM calculations are presented in Table 3. They were designed in such a way in order to analyze the influence of the reinforcement ratio and the mechanical properties of reinforcing steel on a distribution of cracks in the member of the shear span-to-depth ratio a/d = 2.5 (as during the experiment) and in the short member of a/d = 1.8.

The ANSYS software libraries were used in FEM calculations. A solid FE with eight nodes were used in concrete modeling. Translation in the nodal x, y, and z directions was possible at each node of the solid element. In the three axes of the orthogonal system, the description of cracking, crushing, and plastic behavior of the concrete was used in the solid FE. At the integration points, the stress and strain components were calculated. A discrete model was used to model the steel bars. The reinforcement was characterized by a 3D

bar FE. The connection between the concrete and the steel bar was established as identical displacement in the joined nodes.

Table 3. Members considered in FEM analysis.

Beam	l_{eff} (m)	a/d	Longitudinal Reinforcement			
			Steel Bars	Reinforcement Ratio ρ (%)	Yield Stress f_y (MPa)	Tensile Strength f_t (MPa)
S3k	1.1	2.5	2ϕ18	1.8	453	698
PII-3	1.1	2.5	2ϕ12	0.9	548	654
S1k	0.9	1.8	2ϕ18	1.8	453	698
PII-1	0.9	1.8	2ϕ12	0.9	548	654
PI-1	0.9	1.8	2ϕ18	1.8	548	654

The rectangular mesh was used in the beams models, as it is recommended in the solid FE analysis. The FEM mesh for the S3k and PII-3 beams is shown in Figure 7.

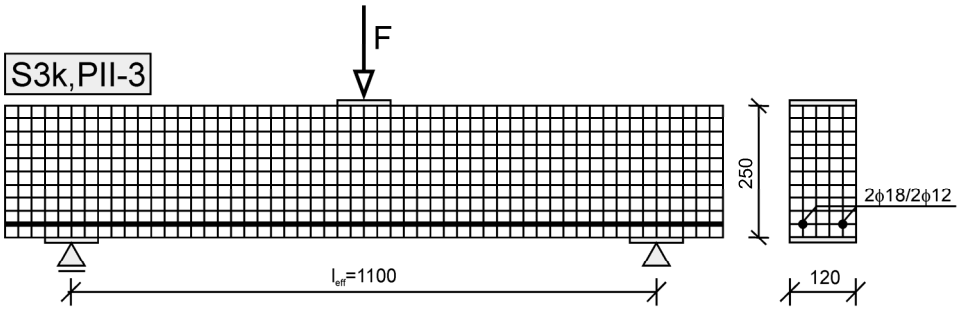

Figure 7. FEM mesh for the beams (unit in mm).

The Willam and Warnke criterion [23] was used to define the concrete limit surface. The criterion enables the use of the concrete nonlinear response in a triaxial stress state and is defined as follows

$$(F/f_c) - S \geq 0, \tag{1}$$

where F is the function of stresses σ_{xp}, σ_{yp}, σ_{zp} in the Cartesian coordinate system direction xyz, S is the surface of failure, and f_c is the uniaxial compressive strength causing crushing. The surface of failure is determined by the principal stresses σ_1, σ_2, σ_3, where: $\sigma_1 \geq \sigma_2 \geq \sigma_3$, σ_1 = max (σ_{xp}, σ_{yp}, σ_{zp}), and σ_3 = min (σ_{xp}, σ_{yp}, σ_{zp}). It also depends on strength characteristics where f_t is the uniaxial tensile strength causing cracking, f_{cb} is the ultimate biaxial compressive strength causing crushing, f_1 is the ultimate compressive strength in biaxial compression state superimposed on the hydrostatic state of stress ${\sigma_h}^a$, and f_2 is the ultimate compressive strength in uniaxial compression state superimposed on the hydrostatic state of stress ${\sigma_h}^a$.

Figure 8 presents the geometrical interpretation of the failure surface. The failure concrete can occur as the cracking state when σ_1, σ_2, or σ_3 is tensile and as the crushing state when each of the principal stresses are compressive. Cracking will occur in the concrete FE when tensile stress in any direction is located outside the surface of failure. In this case, the modulus of elasticity in the direction parallel to the direction of the principal tensile stress will drop to zero. On the other hand, crushing will occur when the three principal compressive stress components are located outside the failure of surface.

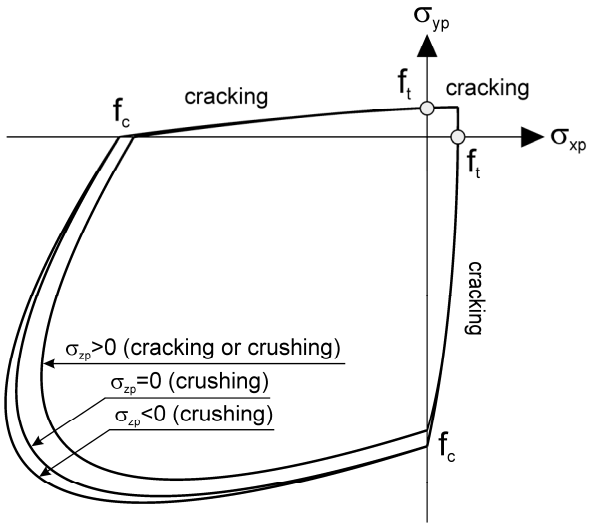

Figure 8. Failure surface with biaxial stress.

During the numerical analysis, nonlinear character of materials was applied. The stress–strain relationship of the concrete in compression was defined by the formulas:

$$\sigma_c = E_c \varepsilon_c / \left[1 + (\varepsilon_c / \varepsilon_{c1})^2\right], \tag{2a}$$

$$\varepsilon_{c1} = 2 f_c / E_c \tag{2b}$$

where: ε_{c1} is the strain at the ultimate compressive strength f_c and E_c is the elastic modulus.

In the stress–strain characteristics for the concrete in tension $\sigma_t - \varepsilon_t$, the tensile softening was included. In the numerical simulation, tensile stress relaxation after cracking was taken into consideration by the stiffness multiplier for the cracked tensile condition $T_c = 0.6$. The hardening effect of the concrete in tension was described by the decreasing linear function of stress depending on R_t. A multiline isotropic hardening material was assigned to steel. The stress–strain relations for concrete in tension and compression are presented in Figure 9, and the steel bars in tension is given in Figure 10.

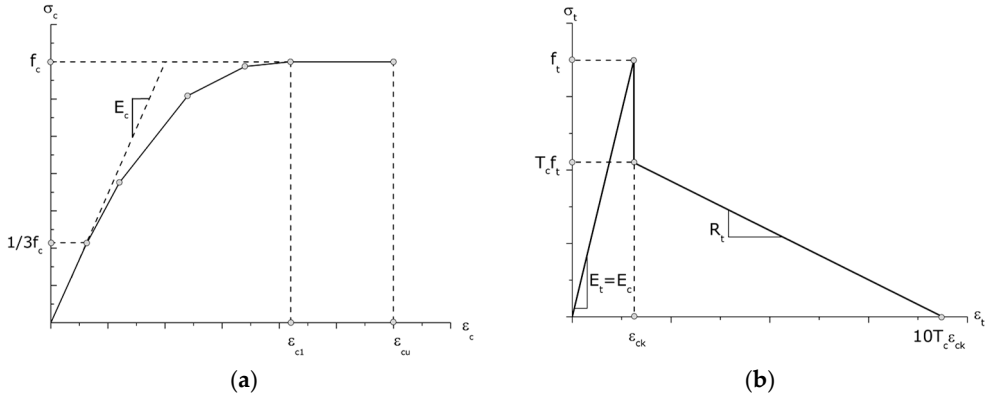

Figure 9. Stress–strain relations for concrete (**a**) in compression; (**b**) in tension.

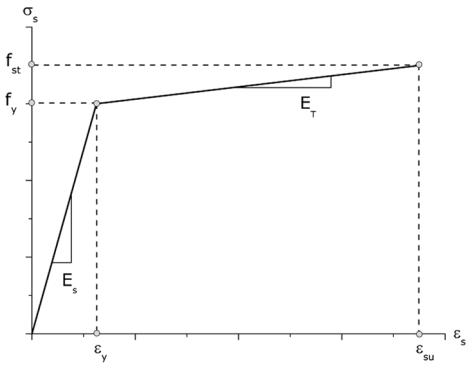

Figure 10. Stress–strain relation for steel reinforcements in tension.

The mechanical properties of concrete under compression and tension have been provided with damage parameters in the numerical model. The stress–strain curves were used in the numerical analysis (see Figure 9). The constitutive model of concrete under compression (see [24]) is presented in Figure 9a and defined by Formulas (2a) and (2b). The key parameters required for the defining of the concrete model are the modulus of elasticity (E_c), compressive strength (f_c), tensile strength (f_t), Poisson's ratio (ν_c), shear transfer coefficients for opened crack (β_t) and for closed crack (β_c), and the stiffness multiplier for the cracked tensile condition (T_c) listed in Table 4. The shear coefficients (β_t, β_c) were introduced as a multiplier to reduce the shear transfer that caused the slip in the plane perpendicular to the crack surface (see also [25]). The mechanical properties of the steel reinforcement defined in the model are presented in Figure 10. The steel reinforcement was treated as an elastic–plastic material with isotropic hardening. The isotropic elastic model was applied for the steel supports. The materials parameters are displayed in Table 4.

Table 4. Materials parameters of the constitutive models for concrete and for steel reinforcement.

Beam	Concrete							Steel Reinforcement			
	E_c (GPa)	f_c (MPa)	f_t (MPa)	ν_c	β_t	β_c	T_c	E_s (GPa)	f_y (MPa)	f_t (MPa)	ν_s
S3k	41.4	35	3.5	0.2	0.1	1.0	0.6	210	453	698	0.3
PII-3									548	654	
S1k									453	698	
PII-1									548	654	
PI-1									548	654	

The Newton–Raphson procedure was used to solve the non-linear problem, as described by Bathe [26], Bonet and Wood [27], Crisfield [28], and Zienkiewicz and Taylor [29]. The following system of numerical equations was applied after the meshing of the model:

$$\mathbf{K}\mathbf{u} = \mathbf{F}^a \tag{3}$$

where $\mathbf{K}$ is the coefficient of the matrix, $\mathbf{u}$ is the vector of the displacement in three directions, and $\mathbf{F}^a$ is the generalized load vector.

The Newton–Raphson procedure performs iterative processes of solving non-linear equations:

$$\mathbf{K}_i^T \Delta\mathbf{u}_i = \mathbf{F}^a - \mathbf{F}_i^{nr} \tag{4a}$$

$$\mathbf{u}_{i+1} = \mathbf{u}_i + \Delta\mathbf{u}_i \tag{4b}$$

where $\mathbf{K}_i{}^T$ is the tangent matrix of stiffness, index i relates to the incremental step number, and $\mathbf{F}_i{}^{nr}$ is the restoring loads vector demonstrating the internal loads of element in the discretized model.

Matrix $\mathbf{K}_i{}^T$ and vector $\mathbf{F}_i{}^{nr}$ were computed based on the displacement vector $\mathbf{u}_i$. More details about the procedure of FEM calculations were presented in [30].

3. Simulation Results and Discussion

Taking into account the dislocations of the nodes and stress components in the global coordinate system obtained as a result of FEM calculations, the trajectories of the total strains were created by the ANSYS program.

The total mechanical strain intensity for two beams corresponding to the tested members, beams PII-3 and S3k of l_{eff} = 1.1, in the subsequent stages of the load are juxtaposed in Figure 11. On the basis of strain distribution, we can make conclusive findings about crack development. When comparing the strain intensity in the same load level in the beams, we can notice some variances in the cracks' evaluation processes depending on the reinforcement ratio, which is very similar as that observed during the experiment. In beam PII-3, with a lower reinforcement ratio, flexural and inclined cracks propagated deeper through the cross section compared to the cracks in beam S3k. The clear differences in strain distribution were also seen when they were juxtaposed in the load stage at failure (see Figure 11). The numerical simulation showed that longitudinal reinforcement affects the process of the cracks' development in the slender beams. However, in the analyzed beams the reinforcement ratio and the yield stress were different, therefore, both parameters could influence the shear capacity and crack distribution.

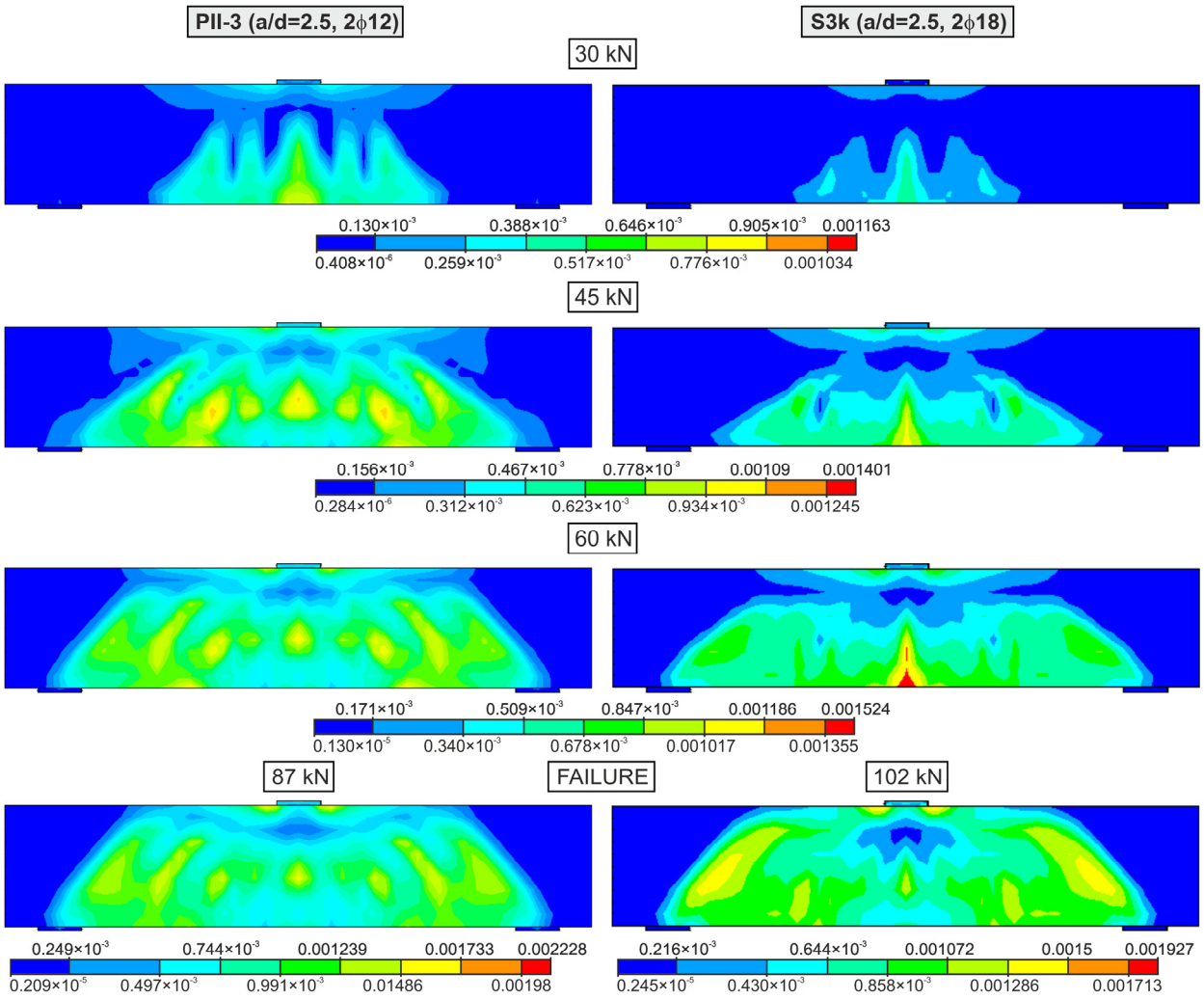

Figure 11. Total mechanical strain intensity for the slender beams PII-3 and S3k.

A good agreement between the strain distribution obtained as a result of numerical analysis and the crack patterns from experiments under ultimate loads, presented in Figure 6, allow us to conclude that the numerical model, which has been applied in the

FEM simulation, can be used for the diagonal crack analysis in non-shear RC beams. The comparison of the load–deflection curves of the experimentally tested and numerically analyzed slender beams PII-3 and S3k is displayed in Figure 12.

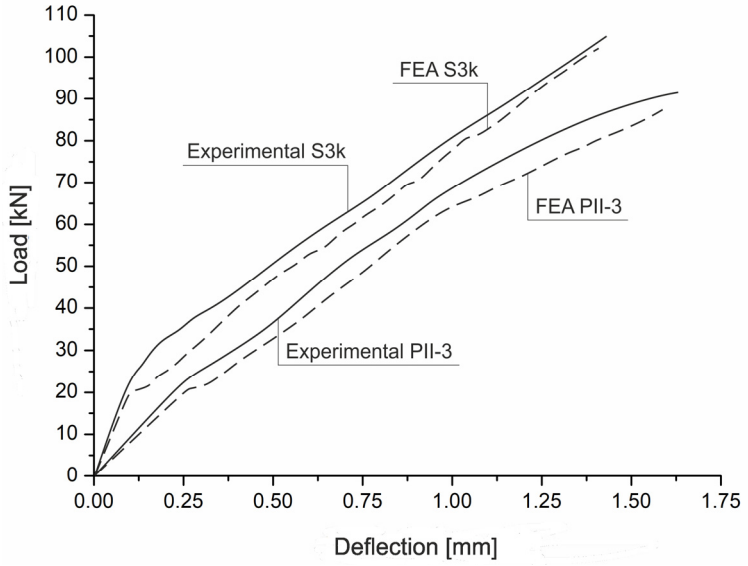

Figure 12. Load–deflection curves. Comparison of FEM results and test results for the slender beams PII-3 and S3k.

The load carrying capacity of both concrete slender beams obtained in the numerical analysis was found to be less than the experimental tests. It was noted that the load–deflection behaviour of both beams was similar in both the experimental and numerical results. The experimental and numerical responses were very similar until the first crack occurred, since the materials were in the elastic stage. The experimental results were not presenting the softening behaviour due to the tests controlled by the load. It can be observed that the ultimate deflection of the tested beams and the numerical results are in good agreement, indicating the maintaining the same serviceability and no loss of ductility.

In the next step of the numerical analysis, the numerical results obtained for beam PII-3 were compared with those for the short beam PII-1. The beams' longitudinal reinforcement consisted of two steel bars ϕ12 mm of the same mechanical properties. To analyze the crack evaluation more precisely in the beams, smeared crack images were evaluated. The development of smeared cracks for beams PII-3 and PII-1 is presented in Figure 13.

When analyzing a smeared cracks evaluation in the slender beam PII-3 (see Figure 13a), it can be seen that the first vertical cracks started to appear in the mid-span of the beam. Following this, with the increase in load and shear stress, some flexural cracks in the shear regions changed their orientation and started to propagate as inclined cracks. A further load increase caused compressive cracks was distinguished just under the load applying. A similar observation of crack evaluation was made during the experiment. The development of smeared cracks in the short beam PII-1 went in a different way (see Figure 13b). Only a few flexural cracks appeared very close to the middle of the span. These cracks propagated slowly in a perpendicular direction. Following this, two main diagonal cracks formed and went directly from the point of the applied force to the supports. The inclined cracks did not develop from flexural cracks. The change in the failure mechanism and a slow development of cracks in the short beam meant that the failure load was significantly higher than in the slender beam. The significantly different view of smeared cracks in the short beam of the shear span-to-depth ratio a/d = 1.8 compared to the smeared cracks distribution in the beam of the shear span-to-depth ratio a/d = 2.5 evidences the transition of failure modes between the short and slender beams reported in the professional literature. It is worth mentioning that the meshless method can be successfully used to simulate the propagation of cracks in reinforced concrete beams under load and directly visualize the failure crack [31,32].

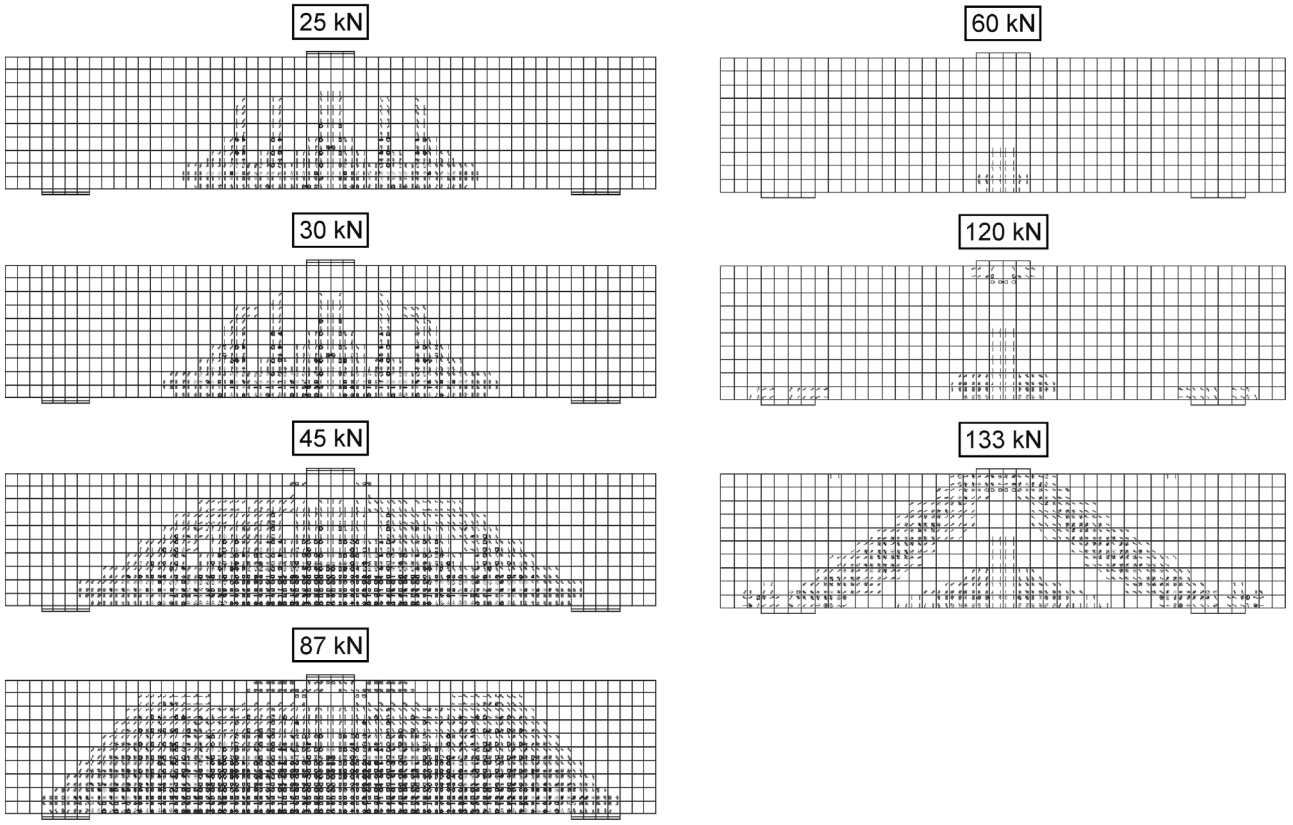

Figure 13. Smeared cracks for the beams (**a**) slender beam PII-3 (a/d = 2.5, ρ = 0.9%, f_y = 548 MPa); (**b**) short beam PII-1 (a/d = 1.8, ρ = 0.9%, f_y = 548 MPa).

In order to analyze whether longitudinal reinforcement influences the crack process in short beams, a comparison of strain intensities obtained during the numerical simulation was made. First, the numerical results obtained for beams PII-1 and PI-1 were juxtaposed (see Figure 14). In these beams, the reinforcement ratio was different (ρ = 0.9% in the beam PII-1 and ρ = 1.8% in the beam PI-1), but the steel bars had the same mechanical properties (f_y = 548 MPa, f_{st} = 631 MPa). Following this, a comparison was performed for beams S1k and PI-1 of the same reinforcement ratio ρ = 1.8% but different steel properties (f_y = 453 MPa, f_{st} = 698 MPa in the beam S1k and f_y = 548 MPa, f_{st} = 631 MPa in the beam PI-1). This comparison is presented in Figure 15.

On the basis of the obtained total strain distributions, the development of following zones can be set apart in short beams: the bending zone in the middle of the span at the beginning of loading, the shear-compression zone near the applied force and in the support regions, and, finally, two shear-compression struts that formed along the loading point and the supports.

When observing the distribution of strain intensity in short beams, it is possible to analyze the progress of crack development. On the basis of the comparison presented in Figure 9, it can be concluded that the cracks that formed in short beams depended on the reinforcement ratio. With the decrease in reinforcement ratio, the process of crack formation was more intensive. The width of the struts was thinner in the beam when the reinforcement was lower. Conversely, a higher reinforcement ratio caused the slower development of struts and less intensive progress of the formation of inclined cracks. Additionally, the mechanical properties of steel bars affected the intensity of the total strain. The comparison presented in Figure 10 shows that the development of struts was quicker in the beam reinforced by steel bars of lower yield stress, which caused faster propagation of inclined failure cracks.

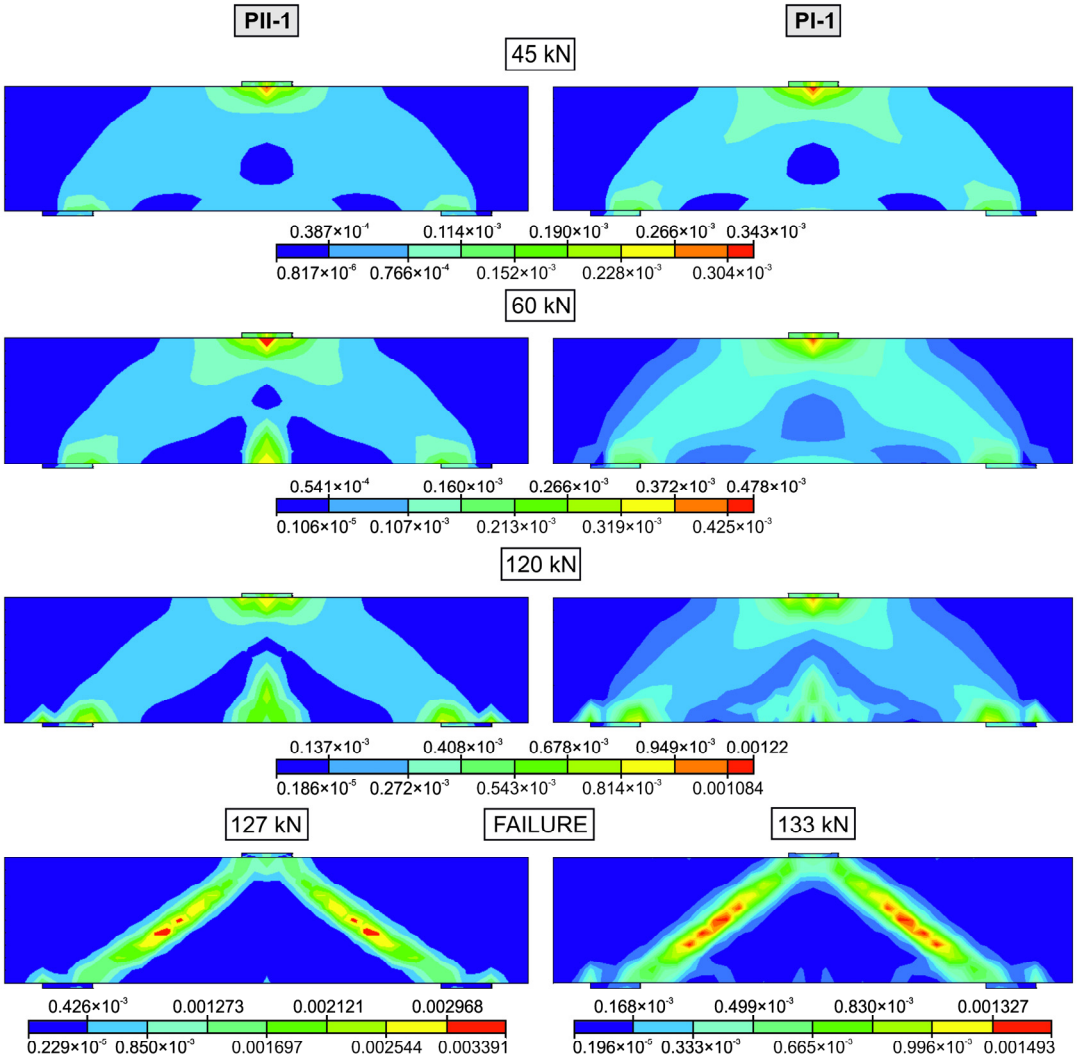

Figure 14. Comparison of strain intensity for the short beams PII-1 (2ϕ12, f_y = 548 MPa) and PI-1 (2ϕ18, f_y = 548 MPa).

The final view of total strain confirmed that the short beams without shear reinforcement can be idealized as a strut and tie system in which the longitudinal reinforcement plays the role of tension tie and thus influences the failure process in these beams.

The numerical results were evaluated using the experimental results of 21 slender RC beams found in the literature [6,22,33,34]. The concrete compressive strength f_c, width b, effective depth d, shear span-to-depth ratio a/d, longitudinal tension reinforcement ratio ρ, and ultimate shear stress v_{ult} were in the range of 23–64 MPa, 0.12–0.15 m, 0.22–0.3 m, 1.5–3.5, 0.8–3.4%, and 1.32–3.43 MPa, respectively. Ultimate shear stresses were calculated as $v_{ult} = V_{ult} / (bd)$, where $V_{ult} = 0.5\,F$. The specimen parameters of the selected experimental data are given in Table 5.

Figure 16 illustrates the ultimate shear stress from FE analyses with increasing shear span-to-depth ratio a/d as compared to the experimental results.

According to Figure 16, the ultimate shear stress of the beam v_{ult} declined with the increase in the shear-span-to-depth ratio a/d and the increasing longitudinal tension reinforcement ratio ρ. This was observed in both physical tests and numerical analyses. The numerical beams had predicted the shearing capacity of the experimental beams (for a/d = 2.5) with good accuracy. The maximum difference between the numerical and experimental ultimate shear stresses was about 15%. On the other hand, the numerical beams with a/d = 1.8 were well in line with the trend in the ultimate shear stress of the

experimental beams tested by Kani [6]. It could be seen that the experimental beams had a very similar tension reinforcement ratio to the numerical beams, but a slightly larger cross-section with a lower concrete compressive strength. It can, therefore, be concluded that the agreement between the numerical and experimental results for beams with a/d = 1.8 is satisfactory.

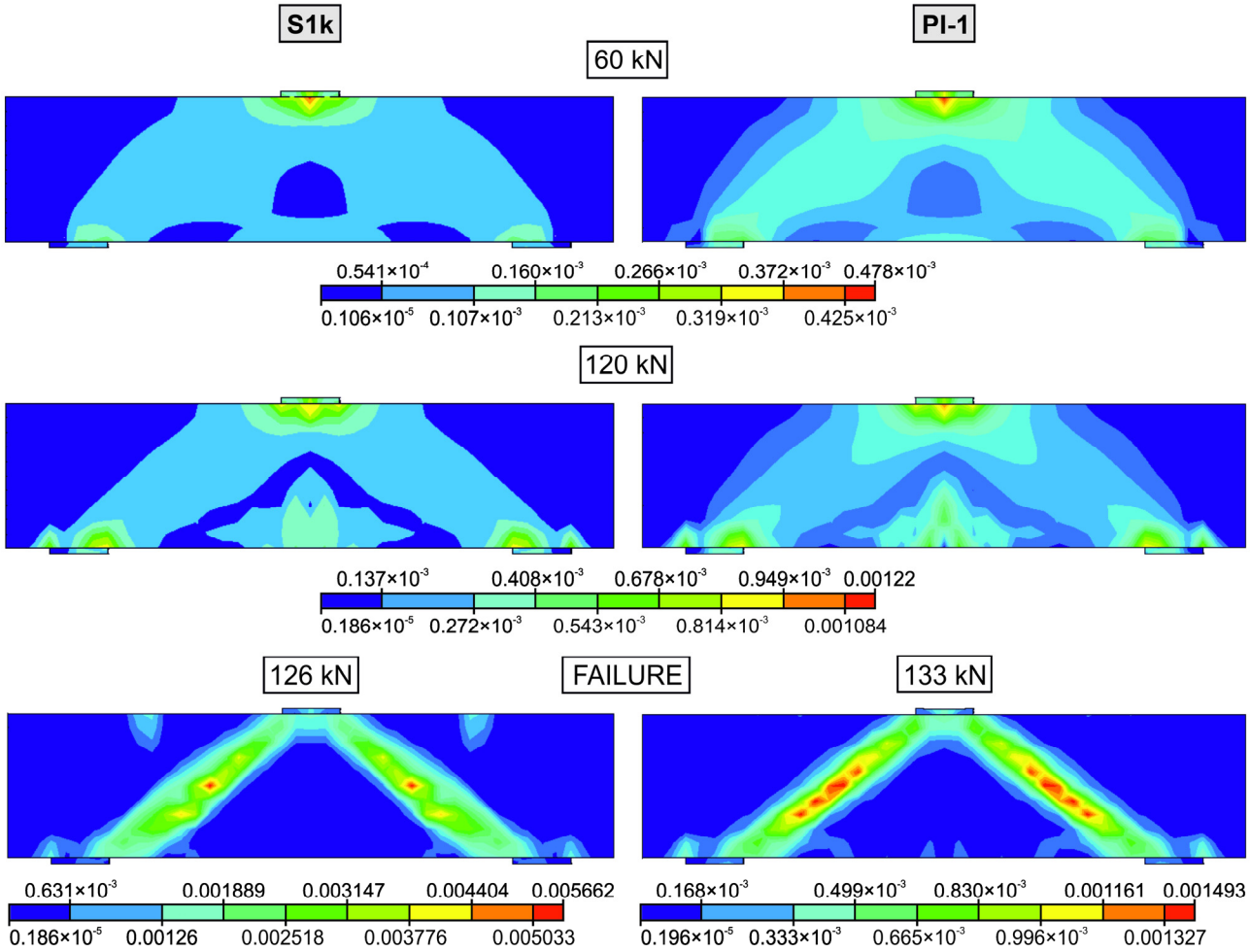

Figure 15. Comparison of strain intensity for the short beams S1k (2ϕ18, f_y = 453 MPa) and PI-1 (2ϕ18, f_y = 548 MPa).

Table 5. Data of test results completed for the comparison.

Source	Number of Specimens	f_c (MPa)	b (m)	d (m)	a/d (-)	ρ (%)	v_{ult} (MPa)
The own FEM results	5	35	0.12	0.22	1.8, 2.5	0.9, 1.8	1.64–2.52
The own experiment	2	35	0.12	0.22	2.5	0.9, 1.8	1.93, 2.12
Shuaib & Lue [22]	3	64	0.13	0.23	2.3, 2.7, 3.0	1.8	1.51–2.68
Mphonde & Frantz [33]	1	23	0.15	0.30	1.5	3.4	2.45
Bukhari & Ahmad [34]	6	48	0.15	0.27	2.0, 2.5, 3.0	0.9, 1.1	1.32–2.85
Kani [6]	11	27	0.15	0.27	1.5, 2.0, 2.5, 3.0, 3.5	0.8, 1.9, 2.8	0.85–3.43

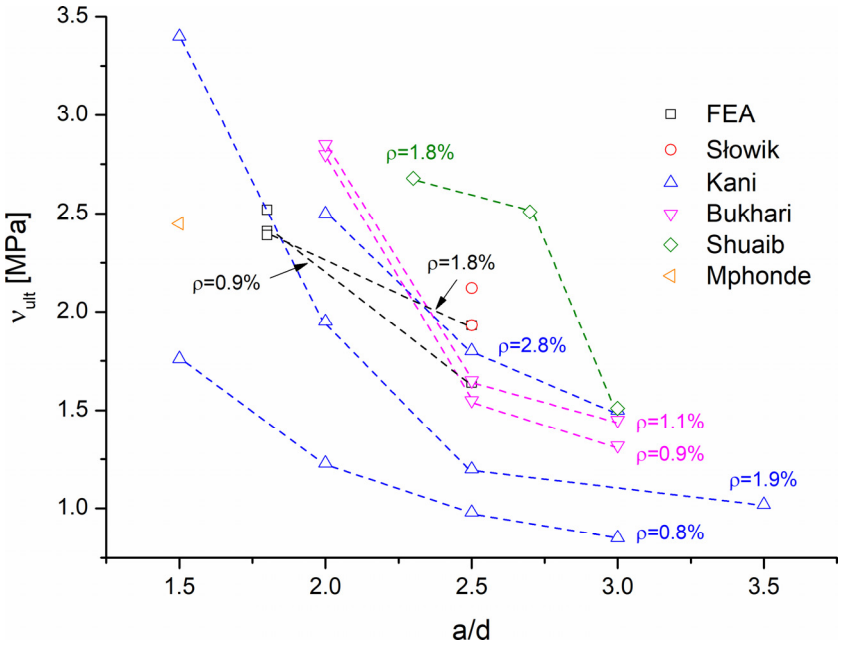

Figure 16. Ultimate shear stress from experiments and FE analyses for varying shear span-to-depth ratio *a/d*.

4. Conclusions

The procedure of FEM calculation, which has been presented in the paper, has been satisfactory verified when performing the simulation of cracking in longitudinally reinforced concrete beams without stirrups. The numerical images of cracks for two beams of the effective length l_{eff} = 1.1 m were successfully compared with the experimental findings. The strain trajectories correctly described the distribution and development of cracks in the beams.

The numerical simulation confirmed that the character of failure process altered according to the shear span-to-depth ratio. In the slender beams of a/d = 2.5, quite a different process of cracking was observed compared to the short beams of a/d = 1.8. This observation gave evidence of the transition in failure modes from the flexure–shear failure in slender beams to the strut and tie model in short beams.

The performed numerical analysis showed that the progress of the flexural and diagonal cracks in the slender beams was significantly faster when the reinforcement ratio was lower. In short beams, the crack evaluation depended on the reinforcement ratio and steel properties as well. It can be concluded that crack distribution is affected by longitudinal reinforcement in both slender and short beams.

Longitudinal reinforcement plays an important role in carrying shear stress in the support zones of the flexural beam, particularly in the member without shear reinforcement. However, the participation in shear carrying is based on a different mechanism. In slender beams, the dowel action of steel bars takes place. In short beams, the stream of stress is formed similar to a strut, which allowed the beam to carry the shear force directly to the supports, with the longitudinal bars acting as a tensile chord.

The process of crack propagation in concrete members that are reinforced longitudinally but do not have stirrups should be wider analyzed according to a different mechanism of carrying shear stress by steel bars in the inclined crack. Further experimental and numerical works are planned to investigate the influences of longitudinal reinforcement and both the ratio and mechanical properties of reinforcing steel on cracking process in slender and short beams.

Author Contributions: Conceptualization, P.S. and M.S.; methodology, P.S and M.S.; software, P.S.; validation, P.S. and M.S.; formal analysis, P.S. and M.S.; investigation, P.S. and M.S.; resources, M.S.; data curation, P.S.; writing—original draft preparation, P.S. and M.S.; writing—review and editing, P.S. and M.S.; visualization, P.S.; supervision, M.S.; project administration, M.S.; funding acquisition, P.S. All authors have read and agreed to the published version of the manuscript.

Funding: This research was funded by "Subvention for Science" (MEiN), project no. FN-4/2023.

Data Availability Statement: The data that support the findings of this study are available from the corresponding author, P.S., upon reasonable request.

Acknowledgments: The authors would like to thank every person/department who helped thorough out the research work. The careful review and constructive suggestions by the anonymous reviewers were gratefully acknowledged.

Conflicts of Interest: The authors declare no conflict of interest.

References

1. Słowik, M. The analysis of failure in concrete and reinforced concrete beams with different reinforcement ratio. *Arch. Appl. Mech.* **2019**, *89*, 885–895. [CrossRef]
2. Walraven, J.C. Fracture Mechanics of Concrete and Its Role in Explaining Structural Behaviour. In *Fracture Mechanics of Concrete and Concrete Structures–High-Performance Concrete, Brick-masonry and Environmental Aspects*; Carpinteri, A., Gambarova, P.G., Ferro, G., Plizzari, G., Eds.; Taylor & Francis Group: London, UK, 2007; pp. 1265–1275.
3. Słowik, M. *Experimental Study of Shear Failure Mechanism in Concrete Beams*; Brittle Matrix Composites 10; IFTR and Woodhead Publishing Limited: Warsaw, Poland, 2012; pp. 345–354.
4. Carpinteri, A.; El-Khatieb, M.; Cadamuro, E. Failure mode transition in RC beams: A cohesive/overlapping crack model application. *Meccanica* **2013**, *48*, 2346–2366. [CrossRef]
5. Arowojolu, O.; Ibrahim, A.; Almakrab, A.; Saras, N.; Nielsen, R. Influence of Shear Span-to Depth Ratio on behavior of High-Strength Concrete Beams. *Int. J. Concr. Struct. Mater.* **2021**, *15*, 14. [CrossRef]
6. Kani, G.N.J. Basic Facts Concerning Shear Failure. *J. ACI* **1966**, *63*, 675–692.
7. Bentz, E.C. Summary of Development and Use of ASA 2004 Shear Design Provisions. In *Advances in Engineering Structures, Mechanics & Construction*; Pandey, M., Wei-Chau, X., Lei, X., Eds.; Springer: Dordrecht, The Netherlands, 2006; pp. 67–80.
8. Keskin, R.S.O.; Arslan, G. Predicting diagonal cracking strength of RC slender beams without stirrups using ANNs. *Comput. Concr.* **2013**, *12*, 697–715. [CrossRef]
9. Słowik, M.; Nowicki, T. The Analysis of Diagonal Crack Propagation in Concrete Beams. *Comput. Mater. Sci.* **2012**, *52*, 261–267. [CrossRef]
10. Bažant, Z.P.; Kim, J. Size Effect in Shear Failure of Longitudinally Reinforced Beams. *ACI J.* **1984**, *81*, 456–468.
11. Bažant, Z.P.; Kazemi, M.T. Size Effect on Diagonal Shear Failure of Beams without Stirrups. *ACI Struct. J.* **1991**, *88*, 268–276.
12. Bažant, Z.P.; Planas, J. *Fracture and Size Effect in Concrete and Quasibrittle Materials*; CRC Press LLC: Boca Raton, FL, USA, 1998.
13. Bažant, Z.P.; Qiang, Y. Designing Against Size Effect on Shear Strength of Reinforced Concrete Beams without Stirrups. *J. Struct. Eng.* **2005**, *131*, 1877–1897. [CrossRef]
14. Carpinteri, A.; Ruiz, C.J.; Ventura, G. Propagation of flexural and shear cracks through reinforced concrete beams by the bridged crack model. *Mag. Concr. Res.* **2007**, *59*, 743–756. [CrossRef]
15. Carpinteri, A.; Corrado, M.; Paggi, M.; Mancini, G. New model for the analysis of size effect on the ductility of reinforced concrete elements in bending. *J. Eng. Mech.* **2009**, *135*, 221–229. [CrossRef]
16. Ma, C.; Guo, Z.; Wang, W.; Qin, Y. Shear Strength Models for Reinforced Concrete Slender Beams: Comparative Analysis and Parametric Evaluation. *Buildings* **2022**, *13*, 37. [CrossRef]
17. Syroka-Korol, E.; Tejchman, J. Experimental investigations of size effect in reinforced concrete beams failing by shear. *Eng. Struct.* **2014**, *58*, 63–78. [CrossRef]
18. Zararis, P.D.; Papadakis, G.C. Diagonal shear failure and size effect in RC beams without web reinforcement. *J. Struct. Eng.* **2001**, *127*, 733–742. [CrossRef]
19. Bentz, E.C.; Buckley, S. Repeating a Classic Set of Experiments on Size Effect in Shear of Members without Stirrups. *ACI Struct. J.* **2005**, *102*, 832–838.
20. Kim, H.G.; Jeong, C.Y.; Kim, M.J.; Lee, Y.J.; Park, J.H.; Kim, K.H. Prediction of shear strength of reinforced concrete beams without shear reinforcement considering bond action of longitudinal reinforcements. *Adv. Struct. Eng.* **2018**, *21*, 30–45. [CrossRef]
21. Słowik, M.; Smarzewski, P. The Study of the Scale Effect on Diagonal Crack Propagation in Concrete Beams. *Comput. Mater. Sci.* **2012**, *64*, 216–220. [CrossRef]
22. Shuaib, A.H.; Lue, D.M. Flexural-Shear Interaction of Reinforced High-Strength Concrete Beams. *ACI Struct. J.* **1987**, *84*, 330–341.
23. Willam, K.J.; Warnke, E.P. Constitutive model for the triaxial behavior of concrete. *Proc. Int. Assoc. Bridge Struct. Eng.* **1975**, *19*, 1–30.
24. Desayi, P.; Krishnan, S. Equation for the Stress-Strain Curve of Concrete. *ACI J. Proc.* **1964**, *61*, 345–350. [CrossRef]

25. Smarzewski, P. Processes of Cracking and Crushing in Hybrid Fibre Reinforced High-Performance Concrete Slabs. *Processes* **2019**, *7*, 49. [CrossRef]
26. Bathe, K.J. *Finite Element Procedures*; Prentice-Hall, Inc.: Upper Saddle River, NJ, USA, 1996.
27. Bonet, J.; Wood, R.D. *Nonlinear Continuum Mechanics for Finite Element Analysis*; Cambridge University Press: Cambridge, UK, 1997.
28. Crisfield, M.A. *Non-Linear Finite Element Analysis of Solids and Structures*; John Wiley & Sons, Inc.: Chichester, UK, 2000.
29. Zienkiewicz, O.C.; Taylor, R.L. *The Finite Element Method for Solid and Structural Mechanics*, 6th ed.; Elsevier Butterworth Heinemann: Oxford, UK, 2006.
30. Słowik, M.; Smarzewski, P. Numerical modeling of diagonal cracks in concrete beams. *Arch. Civ. Eng.* **2014**, *60*, 307–322. [CrossRef]
31. Rabczuk, T.; Belytschko, T. A three-dimensional large deformation meshfree method for arbitrary evolving cracks. *Comput. Methods Appl. Mech. Eng.* **2007**, *196*, 2777–2799. [CrossRef]
32. Rabczuk, T.; Zi, G.; Bordas, S.; Nguyen-Xuan, H. A simple and robust three-dimensional cracking-particle method without enrichment. *Comput. Methods Appl. Mech. Eng.* **2010**, *199*, 2437–2455. [CrossRef]
33. Mphonde, A.G.; Frantz, G.C. Shear Tests of High– and Low–Strength Concrete Beams Without Stirrups. *ACI J.* **1984**, *81*, 350–357.
34. Bukhari, I.A.; Ahmad, S. Evaluation of shear strength of high–strength concrete beams without stirrups. *Arab. J. Sci. Eng.* **2008**, *33*, 321–335.